Human Molecular Genetics, 2020, Vol. 29, No. 7 1107–1120

doi: 10.1093/hmg/ddaa009
Advance Access Publication Date: 21 January 2020
General Article

GENERAL ARTICLE

Structural basis for the dominant or recessive character of *GLIALCAM* mutations found in leukodystrophies

Xabier Elorza-Vidal[1,2], Efren Xicoy-Espaulella[1], Adrià Pla-Casillanis[1], Marta Alonso-Gardón[1], Héctor Gaitán-Peñas[1,2], Carolyn Engel-Pizcueta[1], Juan Fernández-Recio[3,4,5] and Raúl Estévez[1,2,*]

[1]Unitat de Fisiologia, Departament de Ciències Fisiològiques, Genes Disease and Therapy Program IDIBELL-Institute of Neurosciences, Universitat de Barcelona, L'Hospitalet de Llobregat, Spain, [2]Centro de Investigación en red de enfermedades raras (CIBERER), ISCIII, Madrid, Spain, [3]Barcelona Supercomputing Center (BSC), Barcelona, Spain, [4]Institut de Biologia Molecular de Barcelona, CSIC, Barcelona, Spain and [5]Instituto de Ciencias de la Vid y del Vino (ICVV), CSIC- Universidad de La Rioja- Gobierno de la Rioja, Logroño, Spain

*To whom correspondence should be addressed at: Raúl Estévez, Facultat de Medicina, Departament de Ciències Fisiològiques, Universitat de Barcelona-IDIBELL, C/Feixa Llarga s/n 08907 L'Hospitalet de Llobregat, Barcelona, Spain. Tel: (+34) 93 403 9781; Fax: (+34) 93 402 4268; Email: restevez@ub.edu

Abstract

Megalencephalic leukoencephalopathy with subcortical cysts (MLC) is a type of leukodystrophy characterized by white matter edema, and it is caused mainly by recessive mutations in *MLC1* and *GLIALCAM* genes. These variants are called MLC1 and MLC2A with both types of patients sharing the same clinical phenotype. In addition, dominant mutations in *GLIALCAM* have also been identified in a subtype of MLC patients with a remitting phenotype. This variant has been named MLC2B. *GLIALCAM* encodes for an adhesion protein containing two immunoglobulin (Ig) domains and it is needed for MLC1 targeting to astrocyte–astrocyte junctions. Most mutations identified in *GLIALCAM* abolish GlialCAM targeting to junctions. However, it is unclear why some mutations behave as recessive or dominant. Here, we used a combination of biochemistry methods with a new developed anti-GlialCAM nanobody, double-mutants and cysteine cross-links experiments, together with computer docking, to create a structural model of GlialCAM homo-interactions. Using this model, we suggest that dominant mutations affect different GlialCAM–GlialCAM interacting surfaces in the first Ig domain, which can occur between GlialCAM molecules present in the same cell (*cis*) or present in neighbouring cells (*trans*). Our results provide a framework that can be used to understand the molecular basis of pathogenesis of all identified *GLIALCAM* mutations.

Introduction

Leukodystrophies constitute a large group of genetic disorders primarily affecting CNS white matter (1). Within these, Megalencephalic leukoencephalopathy with subcortical cysts (MLC) is characterized by early-onset macrocephaly, epilepsy and cerebral white matter edema (2). It can be caused by mutations in two

Received: December 12, 2019. **Revised:** January 10, 2020. **Accepted:** January 15, 2020

different genes: *MLC1*, which is more frequent (3), and *GLIALCAM* (4). Detailed characterization of MLC patients with *GLIALCAM* mutations revealed two different phenotypes: MLC2A, caused by two recessive mutations and which is indistinguishable from patients containing mutations in MLC1, and MLC2B, caused by one dominant mutation and which shows a remitting, more benign MLC phenotype (2,5).

MLC1 is a membrane protein of unknown functions (6), while GlialCAM is an adhesion molecule that belongs to the immunoglobulin superfamily (7). GlialCAM works as an obligatory subunit of MLC1, being required for MLC1 endoplasmic reticulum exit and targeting to astrocyte–astrocyte junctions (8–10). In addition, GlialCAM is further characterized as an auxiliary subunit of the ClC-2 chloride channel (11), targeting it to cell–cell junctions and modifying its functional properties (12).

Mutagenesis studies determined that the extracellular domain of GlialCAM is required for cell junction targeting, as well as for mediating interactions with itself or with MLC1 and ClC-2 (13). Accordingly, all MLC missense mutations in *GLIALCAM* have been identified in the extracellular domain (2). Within this domain, most missense mutations are located in the first Ig domain (IgV type) and affect GlialCAM localization at cell–cell junctions, observing the same phenotype for mutations identified in MLC2A or MLC2B patients (4,14,15). In contrast, the remaining mutations, which are located in the second Ig domain (IgC2 type), do not affect GlialCAM localization (14).

In order to understand what was the biochemical basis of the genetic character of these mutations, co-expression experiments in primary astrocytes were performed (4). These experiments revealed that the co-expression of GlialCAM wild-type (WT) with GlialCAM containing an MLC2B mutation affected the targeting of GlialCAM WT. In contrast, no effect was observed in GlialCAM WT upon co-expression with GlialCAM containing MLC2A mutations. These effects have been recently validated *in vivo* after the characterization of a knock-in *Glialcam* mice containing the mutation G89S identified in MLC2B patients (9). This mutation affected the targeting of the protein to cell–cell junctions in Bergmann glia, showed vacuoles in the cerebellum in homozygous mice and the heterozygous mice for this mutation showed also a partially altered GlialCAM localization.

All *GLIALCAM* missense mutations studied to date in the first IgV domain reduce the ability of the mutant to interact with GlialCAM WT in the same cell. However, the mutation p.D128N, identified in MLC2B patients, showed an equal ability to interact with GlialCAM WT (14). Thus, a reduced interaction with GlialCAM WT does not sufficiently explain why some mutations behave in a dominant or in a recessive manner. Furthermore, none of the *GLIALCAM* MLC2A or MLC2B mutations identified to date show a decrease in the interaction of GlialCAM with MLC1 or ClC-2, and all GlialCAM mutants are still able to change the functional properties of ClC-2, although its targeting to cell junctions is abolished (14).

So far, there is no evidence to suggest molecular clues that could be used to predict the genetic behaviour of GlialCAM mutants. One puzzling example is that some amino acids have been found containing recessive (the mutation p.R92Q was identified in MLC2A patients) or dominant mutations (the mutation p.R92W was identified in MLC2B patients) (4). Therefore, the molecular basis explaining why a mutation in *GLIALCAM* is recessive or dominant is completely unknown.

In this work, we aimed to understand the biochemical basis that determines why some *GLIALCAM* mutations behave as recessive or as dominant. Using a combination of computational and biochemical approaches, we provide a model for GlialCAM homo-interactions that explains the genetic behaviour of *GLIALCAM* mutations.

Results

Biochemical characterization of newly identified MLC2B GLIALCAM mutations

Previous studies (14) characterized most missense *GLIALCAM* mutations identified in MLC2A and MLC2B patients located in the first IgV domain. These studies indicated that nearly all IgV mutations caused a reduction of the targeting of GlialCAM to cell–cell junctions as well as a reduced ability to interact with GlialCAM WT (as measured by split-TEV assays). An exception was the mutation p.D128N that, despite having a targeting defect, maintained its ability to interact with WT GlialCAM (14).

We characterized in more detail two newly identified MLC2B *GLIALCAM* mutations, p.S59N (2) and p.Q56P (16). Both mutations showed a targeting defect to cell–cell junctions (Fig. 1A and B). Then, we analyzed their ability to interact with GlialCAM WT using split-TEV assays. The experiments showed that mutants p.Q56P and p.S59N maintained the ability to interact with GlialCAM WT, as the mutant p.D128N (14) (Fig. 1C).

Taking these new results into account, we classified mutations affecting residues into the first IgV domain of GlialCAM into three different groups (Fig. 1D): 1) mutants found in MLC2A patients (in green: p.R98C, p.R92Q) that show a reduced ability to interact with GlialCAM WT; 2) a subset of mutants (Dominant 1, D1) found in MLC2B patients (in red: p.G89S/D, p.R92W) with a reduced ability to interact with GlialCAM WT; and 3) a subset of mutants (Dominant 2, D2) found in MLC2B patients (in blue: p.Q56P, p.S59N, p.D128N) which display a normal ability to interact with GlialCAM WT. In a homology model of GlialCAM monomer (see Materials and Methods) (Fig. 1E), D2 mutants were in predicted loops within the same region of the IgV domain, very close in space, despite some of them being far in sequence.

In vitro biochemical assays of the dominant behaviour of MLC2B mutants

To systematically analyze the dominant behaviour of MLC2B mutations, we developed a simple test to determine whether a mutation was acting as dominant in terms of altered trafficking of the WT protein. To achieve this, we transfected HeLa cells with pCDNA3 GlialCAM (WT or containing an MLC2 mutation)-E2A-flag-tagged WT GlialCAM, which allowed the stoichiometric expression of untagged WT/mutant GlialCAM and flag-tagged WT (Fig. 1F, inset). We also co-transfected with MLC1 in order to maximize the cells containing GlialCAM at cell–cell junctions, as previously described (15). We then evaluated the percentage of cells where the flag tagged GlialCAM protein was located at cell–cell junctions by immunofluorescence experiments. These experiments indicated that GlialCAM containing an MLC2A mutation (p.R92Q) did not influence the localization at cell–cell junctions of the flag-tagged WT GlialCAM, whereas GlialCAM containing two different types of MLC2B mutations (p.R92W and p.D128N) reduced the localization of flag-tagged GlialCAM at cell–cell junctions (Fig. 1F). Thus, this newly developed assay was suitable to elucidate whether a GlialCAM mutant was affecting in a dominant manner, the junctional trafficking of the WT protein.

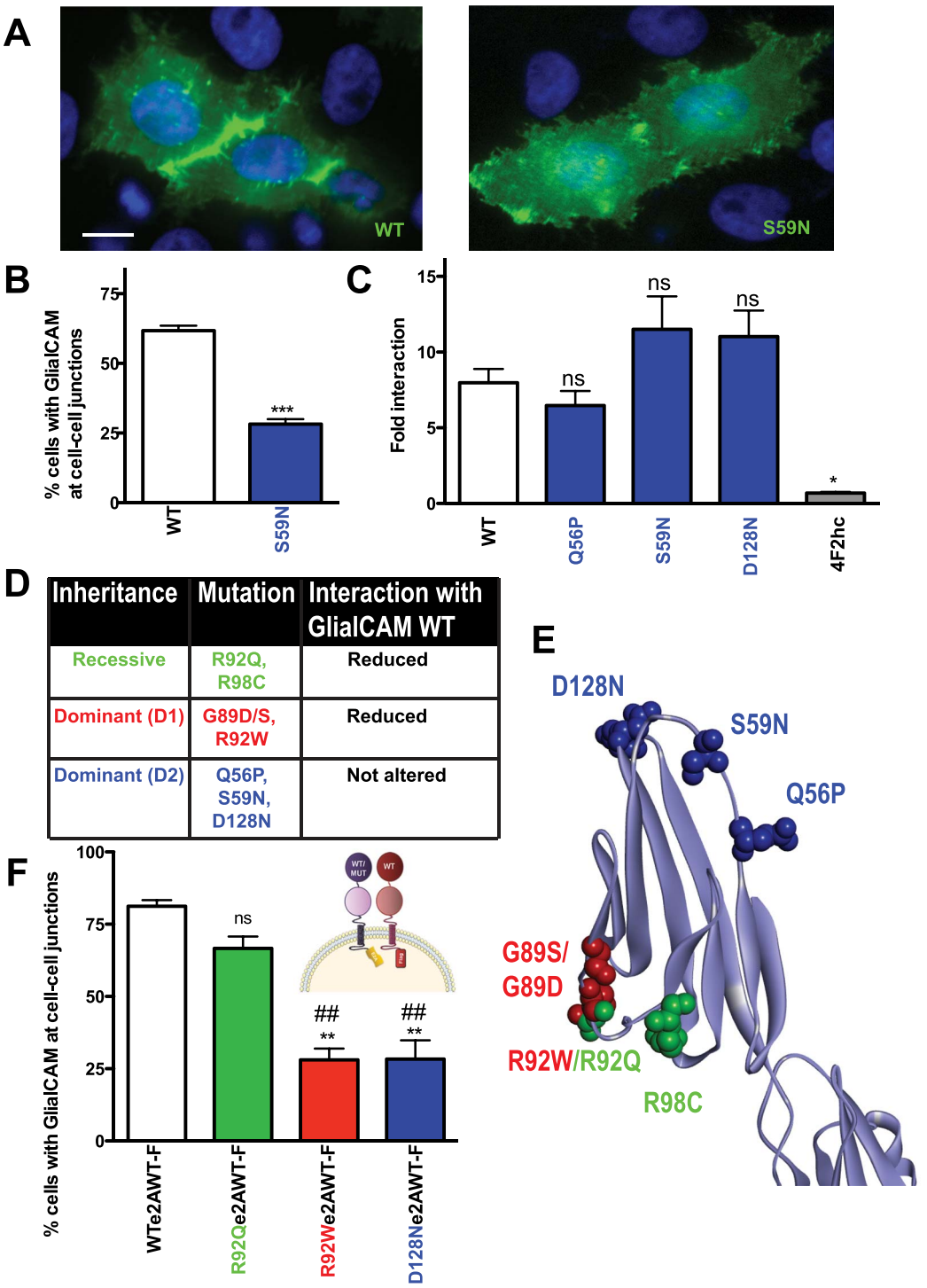

Figure 1. Dominant and recessive MLC2 mutations in *GLIALCAM*. (**A**) Subcellular localization of flag-tagged WT or S59N GlialCAM at cell–cell junctions. Scale bar: 20 µm. (**B**) Quantification of WT and S59N GlialCAM at cell–cell junctions. ***$P < 0.001$ when compared with the WT in paired *t*-student test. Graphics represent mean ± SEM. (**C**) Split-TEV assays of GlialCAM WT interaction with different GlialCAM dominant mutants Q56P, S59N and D128N. Protein 4F2 is used as a negative control of protein interaction. Graphics represent mean ± SEM. ns = non significative, *$P < 0.05$ when compared with GlialCAM WT-WT interaction in Bonferroni multiple comparison's test of five different experiments. (**D**) Classification of GlialCAM IgV mutants according to inheritance (dominant or recessive) and the results of a biochemical assay that measures the level of interaction of the mutants with GlialCAM WT. Mutants are coloured according to this classification. Recessive mutants are coloured in green, dominant mutants (D1) that show a reduced oligomerization in red, and dominant mutants (D2) with a normal oligomerization in blue. (**E**) Three-dimensional homology model of the IgV domain of GlialCAM, with the position of the mutations highlighted. (**F**) Quantification of the percentage of GlialCAM WT cell–cell junction targeting when co-expressed with the GlialCAM WT (130 pair of cells counted) recessive mutant p.R92Q (115 pair of cells) dominant p.R92W (128 pair of cells) or dominant p.D128N (119 pair of cells). Graphics represent mean ± SEM. ns = non-significant, **$P < 0.01$ when compared with co-expression with the WT, ## $P < 0.01$ when comparing dominant mutants with recessive mutant p.R92Q with Bonferroni multiple comparison's test of four different experiments. The inset is a schematic representation of the dominance assay performed, where different GlialCAM proteins (WT or mutant) are co-expressed with flag (F)-tagged GlialCAM WT is achieved by the fusion of both proteins through an E2A peptide.

Characterization of a newly developed nanobody that blocks GlialCAM targeting at cell junctions

As indicated in previous studies (9,13), GlialCAM may form homophilic interactions *in cis* (within the same cell) and homophilic interactions *in trans* (with the neighbouring cell) in order to localize at cell–cell junctions. With the aim of getting information about the regions of the GlialCAM molecule that may be important in mediating *trans* interactions, we developed nanobodies recognizing the extracellular side of GlialCAM. Interestingly, the application of one of the developed nanobodies (Nb 139G1) to cells expressing GlialCAM-VFP blocked the localization of GlialCAM at cell–cell junctions in a concentration-dependent manner (Fig. 2A). In contrast, the application of a control nanobody detecting an unrelated protein at the maximal concentration used did not inhibit GlialCAM localization at cell–cell junctions.

To find which regions of the extracellular domain of GlialCAM were recognized by the nanobody, we expressed GlialCAM with deletions in the IgC2 or in the IgV domain and used flow-cytometry to detect the expressed protein. To normalize for expressed protein at the plasma membrane, we used a monoclonal antibody that detects extracellular GlialCAM. Previous immunofluorescence experiments indicated that both mutant forms (lacking either IgV or IgC2 domain) are expressed at the plasma membrane (13). Deleting the IgC2 reduced partially the binding of the monoclonal and the nanobody (Fig. 2B). In clear contrast, deletion of the IgV domain abolished completely the binding of both antibodies, suggesting that both antibodies mainly bind to the IgV domain (Fig. 2B).

We then tested whether MLC2 GlialCAM mutants affect the binding of the nanobody using flow cytometry. We monitored the binding of the monoclonal antibody as a control of surface expression, which was similar for all our mutants of interest (Fig. 2C for p.Q56P). Interestingly, we observed differences in the binding of the nanobody between the different mutations. We represented the mutants and the effect on nanobody binding in the model of GlialCAM monomer (Fig. 2E). Some mutants, such as p.G89D and p.R98C, decreased binding (Fig. 2D and E). On the other hand, other mutants such as p.R92Q and p.R92W increased binding (Fig. 2D and E). Importantly, mutant p.Q56P was the only that showed completely abolished binding of the nanobody (Fig. 2C–E).

Investigating D2 MLC2B mutants reveal a mechanism of dominance

From our previous results using a nanobody that blocked GlialCAM junctional targeting possibly by inhibiting *trans* interactions, we hypothesized that the region close to residue Q56 may be involved in the formation of these *trans* interactions. Accordingly, we reasoned that mutations p.Q56P, p.S59N and p.D128N, which are all very close in space and are all D2 dominant mutants, may affect specifically *trans* interactions. The replacement of a glutamine by a proline may introduce a kink in the beta-strand. Nonetheless, how mutations p.S59N and p.D128N may affect the structure was unclear.

In western blot experiments, we realized that mutants p.S59N and p.D128N showed a higher motility in SDS gels than the WT protein (Fig. 3A). Analyzing the amino acid protein sequence around the mutation, we noticed that in both cases, the mutations putatively introduced new N-glycosylation sites (Fig. 3B). To prove that this was the case, we compared the motility of GlialCAM WT and these mutants after treatment with Endo Glycosidase-F (Endo-F), which removes all N-glycosylation sites (Fig. 3C). The motility of the mutants in SDS after treatment with Endo-F was equal to the motility of the WT protein, indicating that the mutants in fact introduced a new N-glycosylation site. Thus, we speculate that the new glycosylations created by these mutations might affect specifically *trans* interactions within GlialCAM proteins.

After careful analysis of homologous structures, we identified a possible template for *trans* interactions, between the domains 2 and 3 of contactin (PDB 3JXA) (17). This protein has the highest sequence identity with the GlialCAM extracellular domain (30% SI) (Fig. 3D). Therefore, we built a *trans* dimer by superimposing two copies of the GlialCAM monomer model on contactin domains 2 and 3. In this model, the three mutations studied here mapped to the same interface (Fig. 3E). We therefore conclude that D2 mutations are dominant because they specifically disrupt *trans* interactions between opposed molecules, without interfering with GlialCAM homooligomerization in the same cell.

Experiments toward the development of a structural model of GlialCAM dimers

We further aimed to clarify the molecular basis for the dominance of D1 mutants. As happens in other diseases caused by mutations with both recessive and dominant behaviours (18), we reasoned that the dominant mutations might affect specifically protein contact interfaces of the GlialCAM molecule. As previous studies reported a *cis* dimer orientation that was quite conserved in other members of the CAM family (e.g. nectin-1-EC, CAR) (19), we explored whether GlialCAM could adopt the same *cis* dimeric orientation by superimposing two copies of the monomer model on the corresponding subunits of the CAR dimer.

We first aimed to demonstrate using experimental evidence that the resulting template-based *cis* model may be correct. The model suggested the existence of intermolecular interactions between the pair of residues D129-R92 and R64-E86 (Fig. 4A). We performed directed mutagenesis of these residues to change them to cysteines and expressed in HeLa cells alone or together with the predicted corresponding pair, and the presence of GlialCAM dimers was evaluated by western blot in non-reducing conditions.

Unexpectedly (Fig. 4B), the mutants E86C and R92C formed dimers when expressed alone, independently of the co-expression with the predicted pair. Thus, the cysteine cross-linking experiments invalidated this first structural model based on homology modelling.

As the cross-linking experiments suggested that the glutamate 86 (E86) of one GlialCAM monomer was predicted to be close to the glutamate 86 of the other monomer, we reasoned that other closer residues containing a positive charge might form a positive–negative pair. A closer inspection of the template-based model showed lysine 68 (K68) of one monomer in the vicinity of glutamate 86 (E86) of the other monomer (Fig. 4C), which could be even closer after a small re-arrangement of the dimeric interface. In agreement with the hypothesis that E86 is being stabilized by K68, mutating E86 to arginine (p.E86R) abolished GlialCAM protein expression (Fig. 4D), and its expression was recovered by mutating additionally K68 to glutamate (p.K68E) (Fig. 4D). In contrast, expression was not abolished in the protein containing only the mutation K68E (Fig. 4D) and both mutants (i.e. p.K68E and p.K68E-E86R) showed a defective targeting to cell–cell junctions (Supplementary Material, Fig. S1),

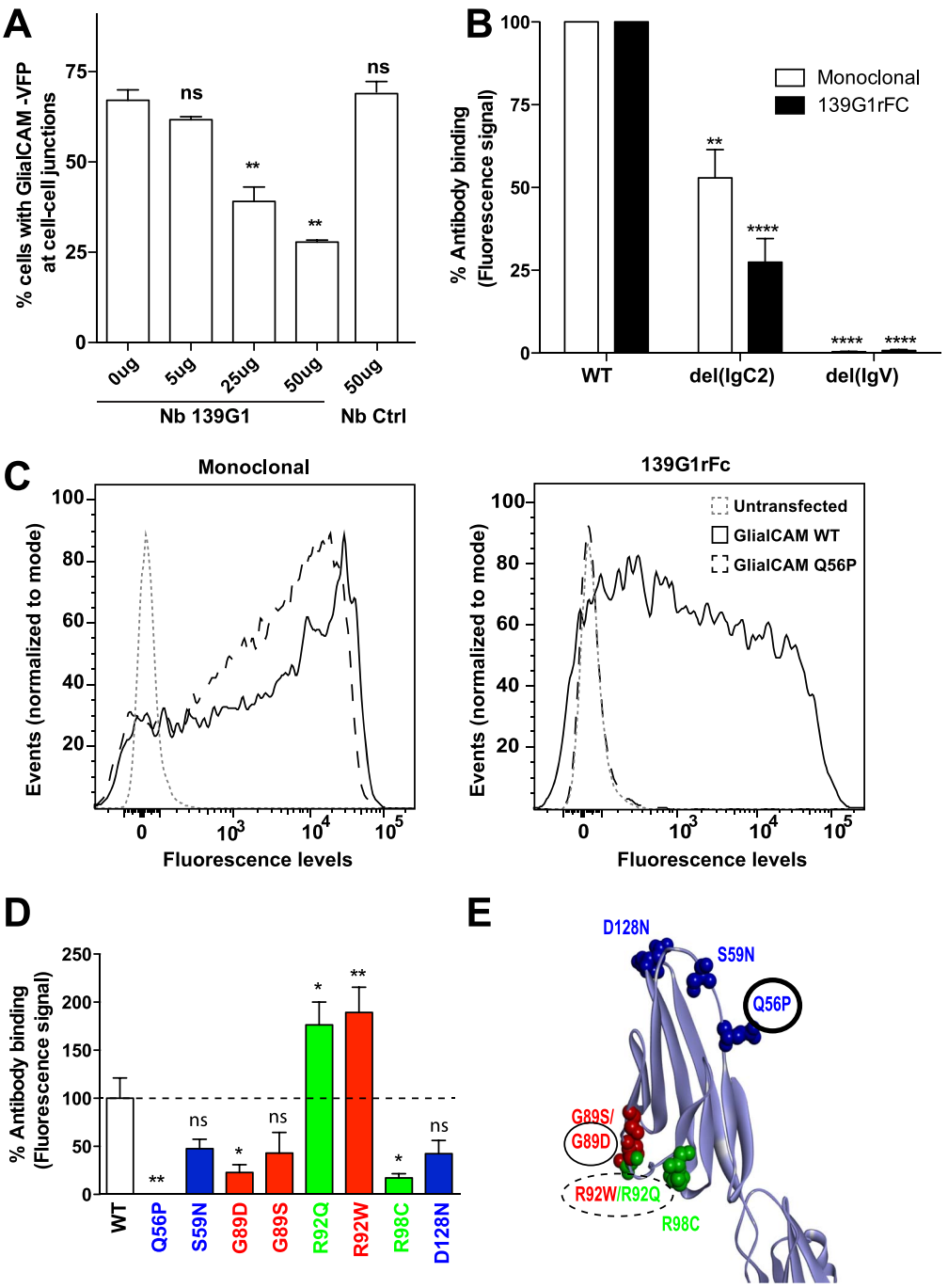

Figure 2. Characterization of a nanobody that blocks GlialCAM localization at cell–cell junctions. (**A**) HeLa cells were transfected with VFP-tagged GlialCAM WT construct and treated with different doses of 139G1 Nb (5, 25 and 50 µg); 181 Nb was used as a negative control. Quantification of the percentage of cells with GlialCAM at cell–cell junctions without Nb was 67.1 ± 2.86% (110 cells), with 5 µg of Nb was 61.7 ± 0.84% (122 cells), 25 µg of Nb was 39.2 ± 4.4% (117 cells), 50 µg of Nb was 27.8 ± 0.5% (111 cells) and 50 µg of Nb control was 68.1 ± 3.4% (104 cells). Graphics represent mean ± SEM. ** $P < 0.01$ in ANOVA Bonferroni multiple comparison test against WT. Data from two independent transfections. (**B**) Quantification of the percentage of antibody binding in HEK293T cells transfected with GlialCAM WT, IgC2 deletion of GlialCAM and IgV deletion of GlialCAM using a flow cytometry assay. Deletions of IgV and IgC2 were performed by PCR resulting in the aminoacid sequence '..TSPVPISRPQV..' for del(IgV) and '..TTVLQGRSLPV..' for del(IgC2). Percentage of antibody binding against del (IgC2) and del (IgV) was normalized with the antibody binding against WT. The mean percentatge of monoclonal antibody (white) against del (IgC2) was 52.8 ± 8.6% ($n = 4$) and against del (IgV) was 0.42 ± 0.07% ($n = 4$). The mean percentage of 139G1 Mb (black) against del (IgC2) was 27.46 ± 7.1% ($n = 4$) and against del (IgV) was 0.74 ± 0.3% ($n = 4$). Graphics represent mean ± SEM. ** $P < 0.01$ ****$P < 0.0001$ in ANOVA Bonferroni multiple comparison test. (**C**) Representative flow cytometry experiments showing the binding of the monoclonal antibody (left) and the 139G1 monobody (right) in untransfected HEK293T cells and cells transfected with WT and p.Q56P GlialCAM. (**D**) Quantification of 139G1 Mb binding by flow cytometry assay in HEK293T cells transfected with different GlialCAM IgV mutants. All the signal of the nanobody for the different GlialCAM IgV mutants were divided by the signal of the monoclonal antibody and normalized with the 139G1 Mb binding against GlialCAM WT. The mean percentage of antibody binding for each mutant was the following: p.Q56P was 0.7 ± 0.4% ($n = 5$); p.S59 N was 47.5 ± 9.9% ($n = 5$); p.G89D was 22.9 ± 8.1% ($n = 4$); p.G89S was 43.1 ± 21.4% ($n = 4$); p.R92Q was 176.3 ± 23.9% ($n = 4$); p.R92W was 189.3 ± 26.3% ($n = 4$); p.R98C was 17.1 ± 4.5% ($n = 3$) and p.D128N was 42.3 ± 13.8% ($n = 5$). Graphics represent mean ± SEM. ns = non-significant; *$P < 0.05$; **$P < 0.01$ in ANOVA Bonferroni multiple comparison test.

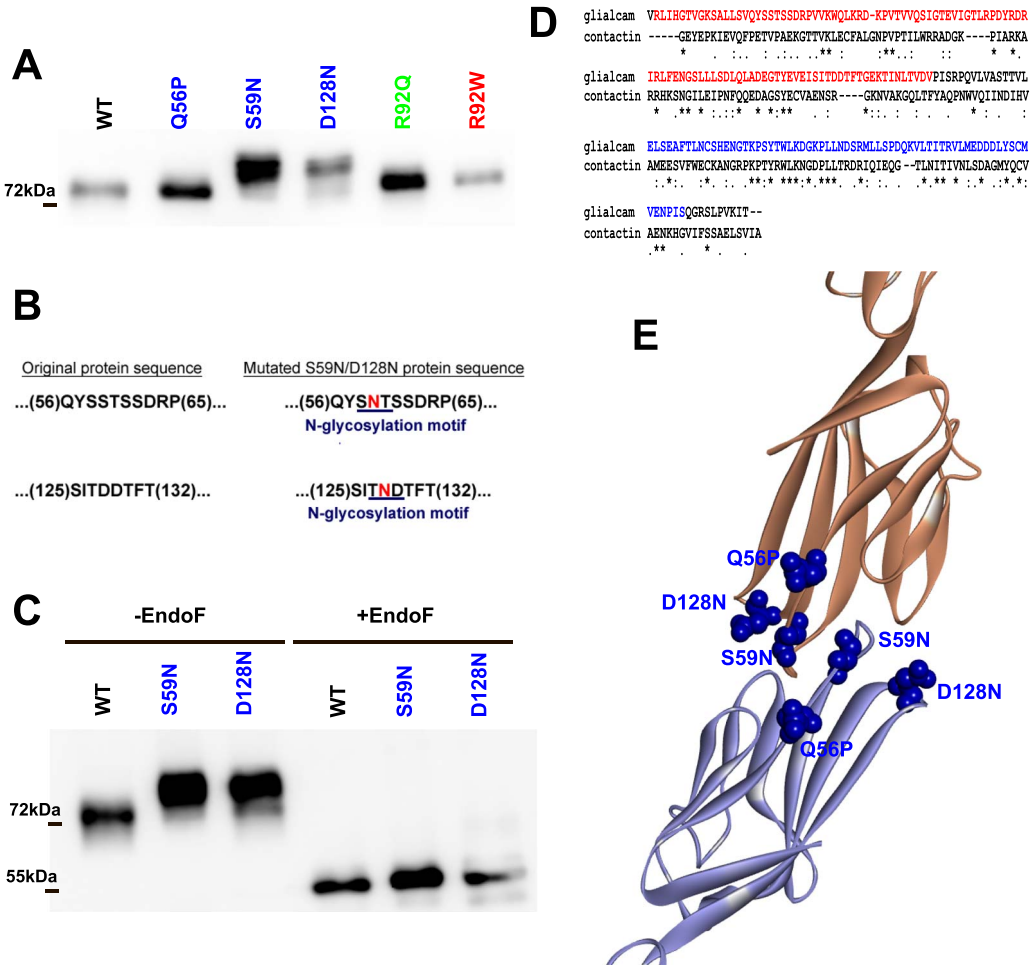

Figure 3. Dominant mutants p.S59N and p.D128N introduce new glycosylation sites in GlialCAM. (**A**) Western blot of transfected cells with flag-tagged GlialCAM WT or carrying dominant or recessive mutations was performed with an antibody detecting the flag epitope. Dominant mutants p.S59N and p.D128N present an increased molecular weight. Another independent experiment gave the same results. (**B**) Predicted *N*-glycosylation motifs that appear in the GlialCAM amino acid sequence due to the p.D128N or the p.S59N dominant mutations. (**C**) Western-blot assay of transfected cells with WT, p.S59N or p.D128N GlialCAM plasmids in control conditions (left) or treated with Endoglycosidase-F (Endo-F) (right) that removes all asparagine-linked mannoses. Treatment with Endo-F results in all GlialCAM constructs presenting the same molecular weight around 50 kDa. Two additional experiments gave the same results. (**D**) Alignment between the Ig domains of contactin and GlialCAM. The IgV domain of GlialCAM is coloured in red and the IgC2 domain in blue. (**E**) Homology model generated to explain the *trans* interaction between the IgV domain of two GlialCAM molecules with key dominant mutants p.Q56P, p.S59N and p.D128N highlighted in blue.

suggesting that E86 may form additional interactions with other residues.

Development of a new structural model of GlialCAM dimerization

Since mutational data and cross-linking experiments did not support the template-based dimer model, we decided to model the *cis* dimer by docking, using the monomer model as input (see Materials and Methods). We selected only docking orientations in which E86 residues from both molecules were within 8 Å distance. From the resulting docking models, the one with the closest E86-K68 distance (6.3 Å) was consistent with all the above mutational data and cross-linking experiments. The new model suggested a large interface formed by the surfaces of the same opposing beta-strands of the IgV domains of two GlialCAM molecules (Fig. 5A, dotted-rectangle in yellow). The interacting segment was formed by residues ranging from Glutamate 86 (E86, in the top) to Arginine 92 (R92, in the bottom) of each GlialCAM molecule (Fig. 5A). To test if this segment (beta strand) from each GlialCAM monomer was interacting in the dimer, we generated new cysteine mutants from the residues of this strand (Isoleucine 88 (I88), Threonine 90 (T90), Leucine 91 (L91)). As a control, we generated the cysteine mutant of Glutamine 81 (Q81), which is also very close, but it is not predicted to be interacting. After expressing these mutants in HeLa cells, we analyzed the formation of GlialCAM dimers by western blot (Fig. 5B). We observed the dimer formation between the pairs of residues E86, I88, T90, L91 and R92, but not with Q81. Treating the extracts with reducing agents (DTT) disrupted the dimers, further confirming that dimers of the cysteine mutants were formed by disulphide bonds (Fig. 5B). In summary, these experiments indicated that the residues from positions 86 to 92 form a specific GlialCAM–GlialCAM interacting segment.

As an additional test that this segment was interacting, we reasoned that introducing a glycosylation site in that segment might work as a dominant mutation. Mutation I88N (Fig. 5C), which increased the motility of GlialCAM because it introduces a new glycosylation (Fig. 5C, inset), caused a dramatic reduction of GlialCAM WT targeting to cell junctions (Fig. 5D). As a control,

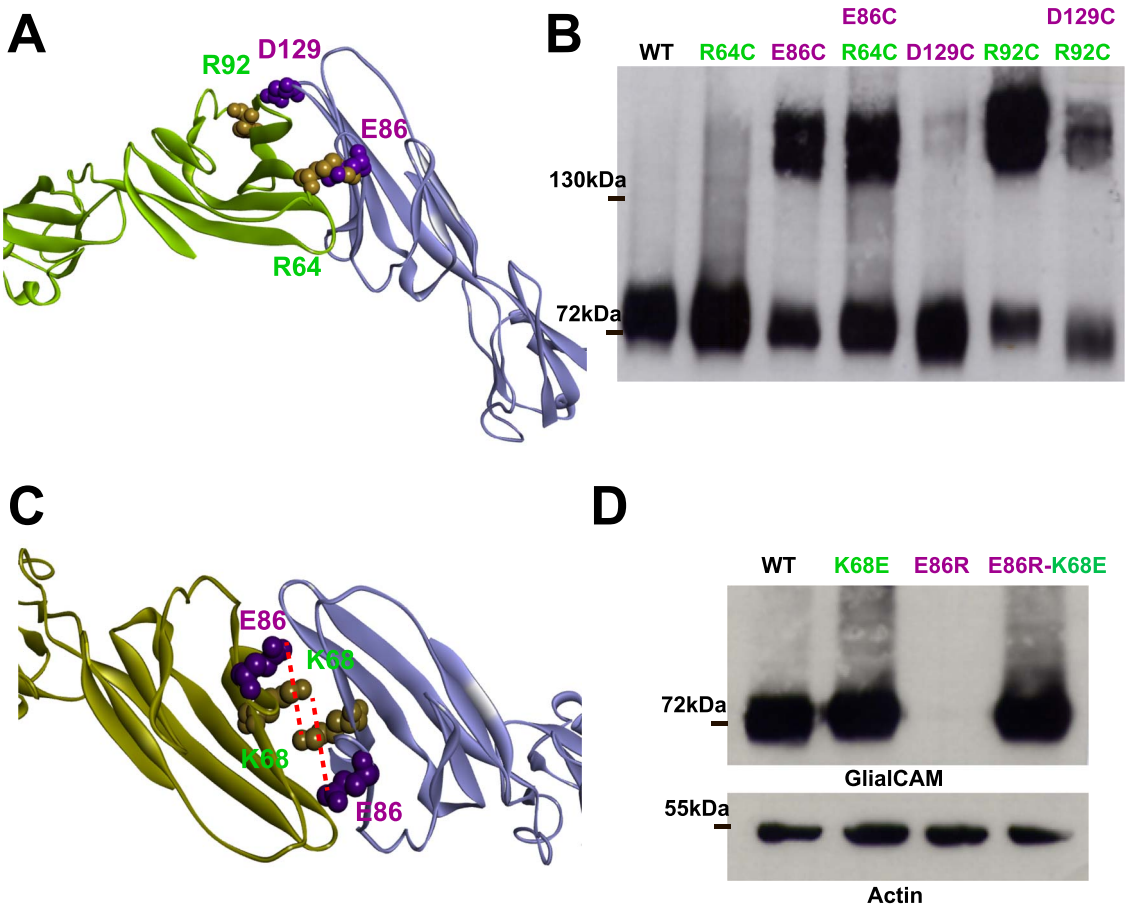

Figure 4. Development and biochemical testing of a structural domain of GlialCAM *cis*-homooligomerization. (**A**) Three-dimensional model of GlialCAM generated by homology modelling using another IgCAM molecule as a template. Possible pairs of interacting residues R64-E86 and R92-D129 are highlighted in orange/purple colours. (**B**) Western blot of GlialCAM WT or mutants changed to Cysteine R64C, E86C, D129C and R92C expressed alone or co-transfected in pairs (R64C + E86C and D129C + R92C) performed to observe Cysteine cross-linked dimerization between the two-paired mutants. Mutants E86C and R92C alone show dimerization, as observed at the 140 kDa band. Representative western blot from three independent experiments. (**C**) Structural representation of the negatively charged residue E86 in the IgV dimer interface. Structural analysis revealed the positively charged residue K68 in the vicinity of E86, which could be even closer after a small interface rearrangement. (**D**) Western blot of transiently transfected cells with GlialCAM WT, K68E mutant, E86R mutant or GlialCAM carrying both aminoacid changes K68E and E86R. While E86R is not expressed, double mutant E86R + K68R protein levels are recovered and similar to protein levels of GlialCAM WT. Data shown are from a representative experiment, out of three independent ones. Actin was used as a loading control.

mutation P76N (Fig. 5C), which also introduces a glycosylation site, reduced only slightly the targeting of GlialCAM WT to cell junctions (Fig. 5D).

Additional characterization of cysteine mutants in the interacting segment provide new keys to differentiate dominant and recessive mutants

We additionally assessed if these cysteine mutants from the GlialCAM interacting segment showed a defect in the targeting to cell–cell junctions (Fig. 6A). Unexpectedly, compared with GlialCAM WT expressed alone, mutant E86C showed an increased targeting to cell–cell junctions, reaching the same values of the co-expression of GlialCAM plus MLC1 (Fig. 6A) (15). In contrast, all the other cysteine mutants (I88C, T90C, R91C and R92C) showed a defect in the targeting to cell–cell junctions.

Given these results, we reasoned that mutation E86C might stabilize the GlialCAM dimer in a more stable conformation, which will result in an increased targeting of the mutant to cell–cell junctions. Then, we decided to explore whether the introduction of the mutation E86C might reverse the trafficking defect caused by recessive or dominant mutations. It was found (Fig. 6B) that the E86C mutation rescued almost completely the trafficking defect caused by the recessive mutation p.R92Q, while it did not increase the targeting of dominant mutants (D1 (p.R92W) and D2 (p.S59N)) to cell junctions (Fig. 6B).

Analyzing the structural mechanism of dominance of some MLC2B mutations

From all *GLIALCAM* mutations identified in MLC2B patients, those affecting their interaction with GlialCAM (i.e p.G89S/D, p.R92W) are found in the identified *cis*-dimerization interacting segment. In contrast, all the MLC2A mutations except p.R92Q are found outside of this segment (p.K68M, p.R98C, p.T132N), suggesting that mutations located in this specific segment will be dominant. To understand the behaviour of the residue R92, we constructed several mutants of this residue to different amino acids, co-expressed them with GlialCAM WT (Fig. 7A) and analyzed whether they behave in a dominant or recessive manner regarding the targeting of GlialCAM WT. Mutation of R92 to the small amino acid alanine (A) did not result in a significant dom-

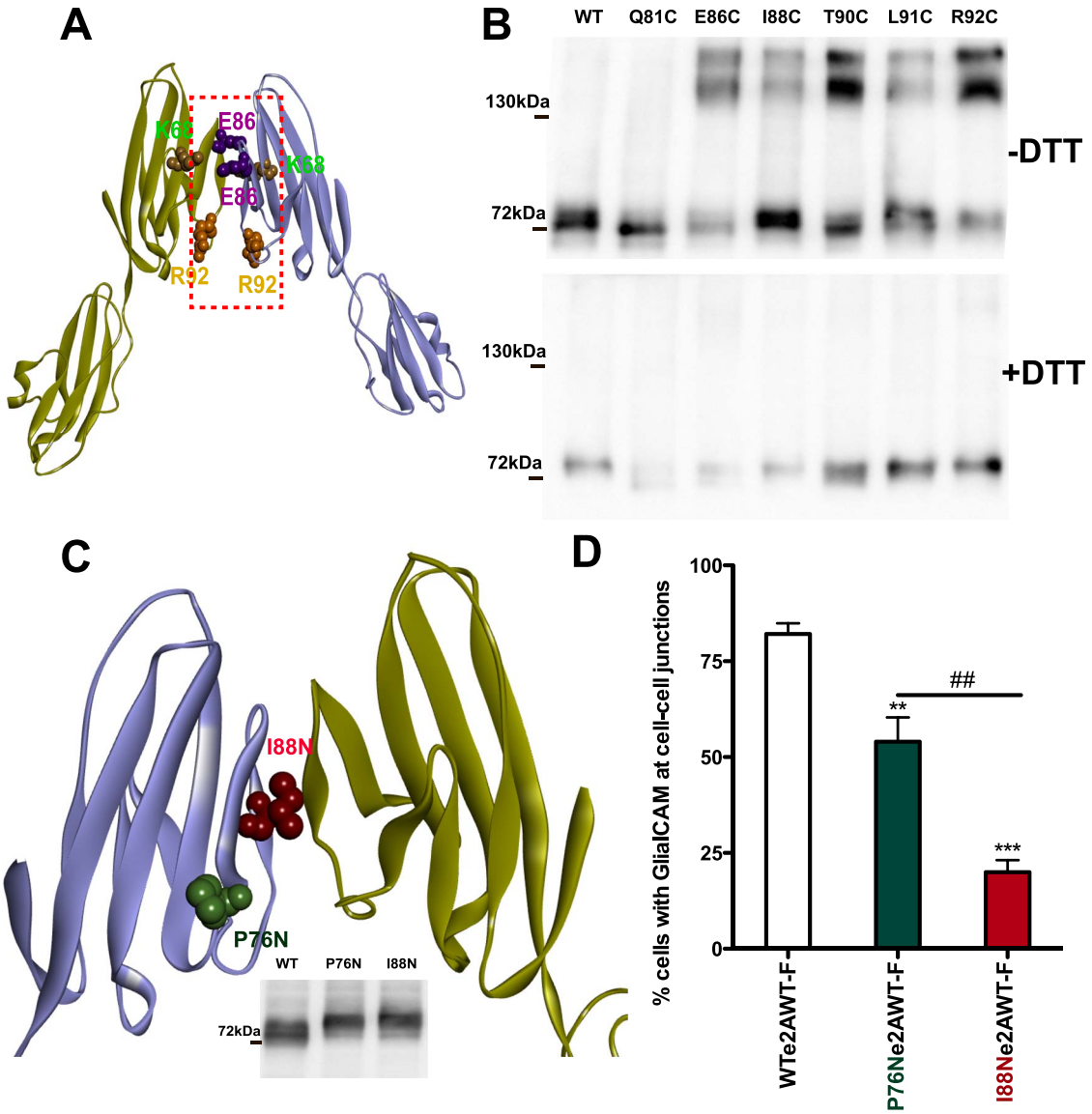

Figure 5. Three-dimensional model of GlialCAM homo-dimerization based on docking. (**A**) Structural representation of the new structural model of GlialCAM dimer based on docking analysis after applying several constraints based on the results from biochemical studies. The interacting surface between the two IgV domains is highlighted in yellow (left). Residues E86 and R92 are paired in close proximity and residue K68 is also highlighted. (**B**) Western-blot assay of cysteine cross-link in the absence or in the presence of 100 mM DTT between the following residues mutated to cysteine: Q81C, E86C, I88C, T90C, L91C and R92C. GlialCAM WT is used as a negative control. Dimers are observed on the mutants E86C, I88C, T90C, L91C and R92C at 140 kDa. Representative western-blot of three independent experiments. (**C**) Scheme of the IgV interaction showing the position of the introduction of two different glycosylation sites, I88N in the interacting segment and P76N as a control. The inset shows a western blot of transfected cells with flag-tagged GlialCAM WT or carrying the introduced glycosylation sites detected with an antibody detecting the flag epitope. Both P76N and I88N present an increased molecular weight. Another experiment gave the same results. (**D**) Biochemical dominance assay of GlialCAM WT targeting to cell–cell junctions co-expressed with different glycosylation mutants. Quantification of flag-tagged GlialCAM at cell–cell junctions (right) when co-expressed in E2A constructs with GlialCAM WT (232 cells), mutant P76N (174 cells) and mutant I88N (176 cells). Graphics represent mean ± SEM. $^{**}P < 0.01$, $^{***}P < 0.001$ when compared with co-expression with the WT. In addition, we also compared with the mutant P76N, to distinguish better between recessive and dominant effects. $^{\#\#}P < 0.01$ when comparing I88N with mutant P76N in Bonferroni multiple comparison's test of three–four different experiments.

inant effect, whereas mutation to tryptophan (W) or tyrosine (Y) was dominant (Fig. 7A). Interestingly, mutants R92 to aspartate (D) or cysteine (C) were also dominant (Fig. 7A). We hypothesized that the dominant mutants of this residue may have the ability to form novel interactions around this region, maybe distorting the native dimer orientation.

By inspecting in the new dimer model residues near to the position of R92 in the other monomer, we found R96 (Fig. 7B). To test the putative interaction of R92 mutants with R96, we focused on the mutant R92D and then constructed the single mutant R96D and the double mutant R92D/R96D and assayed its localization at cell–cell junctions (Fig. 7C). Both R92D and R96D mutants showed a defective targeting to cell–cell junctions (Fig. 7C). In contrast, the double mutant R92D-R96D was targeted to cell junctions as the WT protein.

In summary, our results suggest that there is an interaction segment between residues E86 (located on the top of the beta strand) and R92 (found in the bottom) (Fig. 7D). Although residues E86 from each dimer are close, they are stabilized by its interaction with K68. In the bottom edge, opposed residues

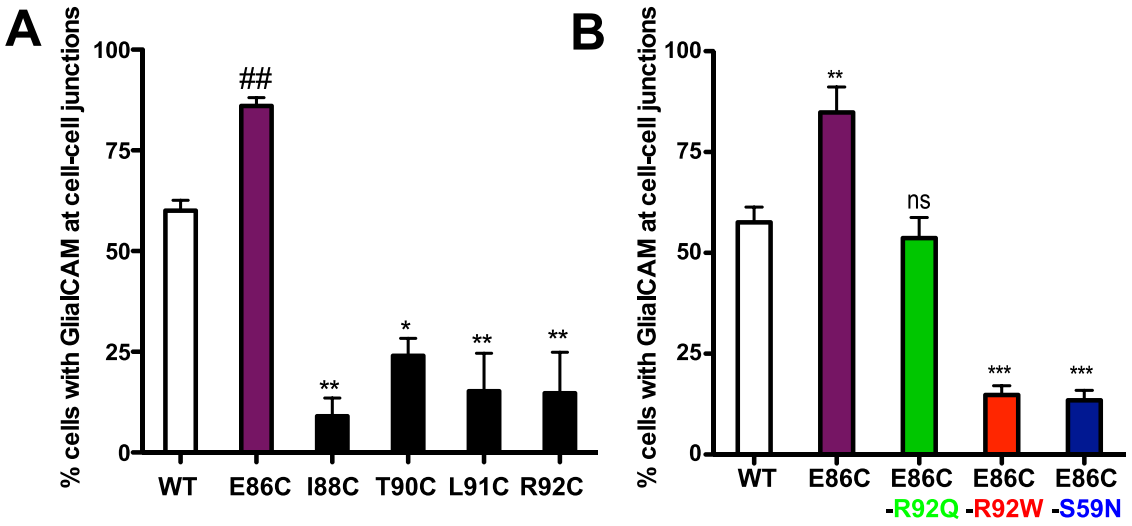

Figure 6. Characterization of the trafficking to cell junctions of GlialCAM cysteine mutants in the interacting segment. (**A**) Percentage at cell–cell junctions of GlialCAM E86C (230 cells) I88C (177 cells) T90C 185 cells) L91C (123 cells) and R92C (91 cells) compared with GlialCAM WT (198 cells). Graphics represent mean ± SEM. $^{*}P < 0.05$, $^{**}P < 0.01$ in Bonferroni multiple comparison test versus WT of three independent experiments. $^{\#\#}P < 0.01$ in T-student test compared with WT in data from four independent experiments. (**B**) Quantification of percentage of cells with GlialCAM in cell junctions for WT (101 cells) E86C (94 cells), E86C-p.R92Q (356 cells), E86C-p.R92W (137 cells) and E86C-p.S59N (147 cells). Graphics represent mean ± SEM. $^{**}P < 0.01$ and $^{***}P < 0.001$ in Bonferroni multiple comparison test, compared with WT. Data from three independent experiments.

R92 may be slightly separated through electrostatic repulsion with R96 (Fig. 7D). The mutation of R92 by charged aspartate can introduce favourable salt bridge with R96 of the other monomer, bringing to a close vicinity this bottom region that in principle was slightly separated in the native protein. Similarly, the introduction of aromatic residues (tryptophan or tyrosine) could introduce novel cation-pi interactions with R96, producing similar effect. The dominant effect of R92C might also be explained by the formation of dipole–dipole interactions or by a disulphide bridge, suggesting that GlialCAM may form oligomers of dimers by lateral interactions (see Discussion). Thus, we speculate that residues in this segment that create aberrant neo-interactions, which might be inducing a different dimer orientation, may be dominant.

Discussion

Our aim was to understand why missense mutations from the first Ig domain (IgV), which are found in MLC2 patients, differentially behave as dominant or recessive. The study of most MLC2B missense dominant mutations that have a trafficking defect has revealed that they can be classified in two groups taking into account regarding whether they display or not a reduced ability to interact with the WT protein. Locating both types of MLC2B mutations in a structural model of the extracellular domain of GlialCAM protein developed in the present work, which takes into account homologous structures, docking energetics and biochemical experiments (Fig. 8), suggested that both types of MLC2B mutations affect GlialCAM-GlialCAM interacting interfaces. In one case (D1), they may affect to interactions involved in GlialCAM–GlialCAM *cis* interfaces, whereas for the other group of mutants (D2), they allegedly affect interactions involved in GlialCAM–GlialCAM *trans* contacts. As it has been shown in other IgCAM molecules (20,21), GlialCAM dimers may be formed first in the endoplasmic reticulum through *cis* mediated interactions that then will travel to the plasma membrane where *trans* interactions may occur. We suggest that MLC2B mutants that showed normal ability to interact with GlialCAM WT may disrupt specifically GlialCAM–GlialCAM *trans* mediated interactions, for instance as in the case of the mutants p.S59N and p.D128N, by creating a new glycosylation site in the mentioned *trans* interaction surface. Possibly, mutant p.Q56P may also disrupt this interaction surface, as proline has a restricted degree of freedom.

Furthermore, GlialCAM is also able to form heterophilic *cis* interactions with MLC1 or ClC-2. It has been previously shown that, although GlialCAM alone reach cell–cell junctions, co-expression with MLC1 increases the percentage of GlialCAM present at cell–cell junctions. Here, we have found a mutant, E86C that also improves the ability of GlialCAM to reach cell–cell junctions. Based on these studies, we suggest that MLC1 may stabilize GlialCAM at cell–cell junctions by changing the conformation of GlialCAM to a similar configuration as the one caused by the mutation E86C.

We analyzed whether mutation E86C could stabilize MLC2A and MLC2B mutants. As the MLC2B p.S59N mutant was not rescued by E86C, we suggest that mutants E86C and p.S59N influence GlialCAM stability by different mechanisms. Contrarily, the double mutant containing E86C and the MLC2A recessive mutation p.R92Q showed a normal targeting to cell–cell junctions, but the double mutant E86C-R92W failed to reach cell–cell junctions. We believe that the MLC2B mutant p.R92W may destabilize *cis* interactions in a different manner than the MLC2A mutant p.R92Q, probably by creating novel interactions, as our experiments with the double mutant R92D-R96D suggest. MLC2B mutant p.R92W may also form novel cation-pi interactions with the residue R96. Thus, we conclude that MLC2B mutants affecting GlialCAM homooligomerization may affect the interacting segment by disrupting extensively the normal pattern of interactions in this segment, as for example, by creating new interactions or by affecting several interactions simultaneously. Using this model, for instance, we could explain why the recently identified p.R92P mutation in MLC2B Chinese patients (22) may

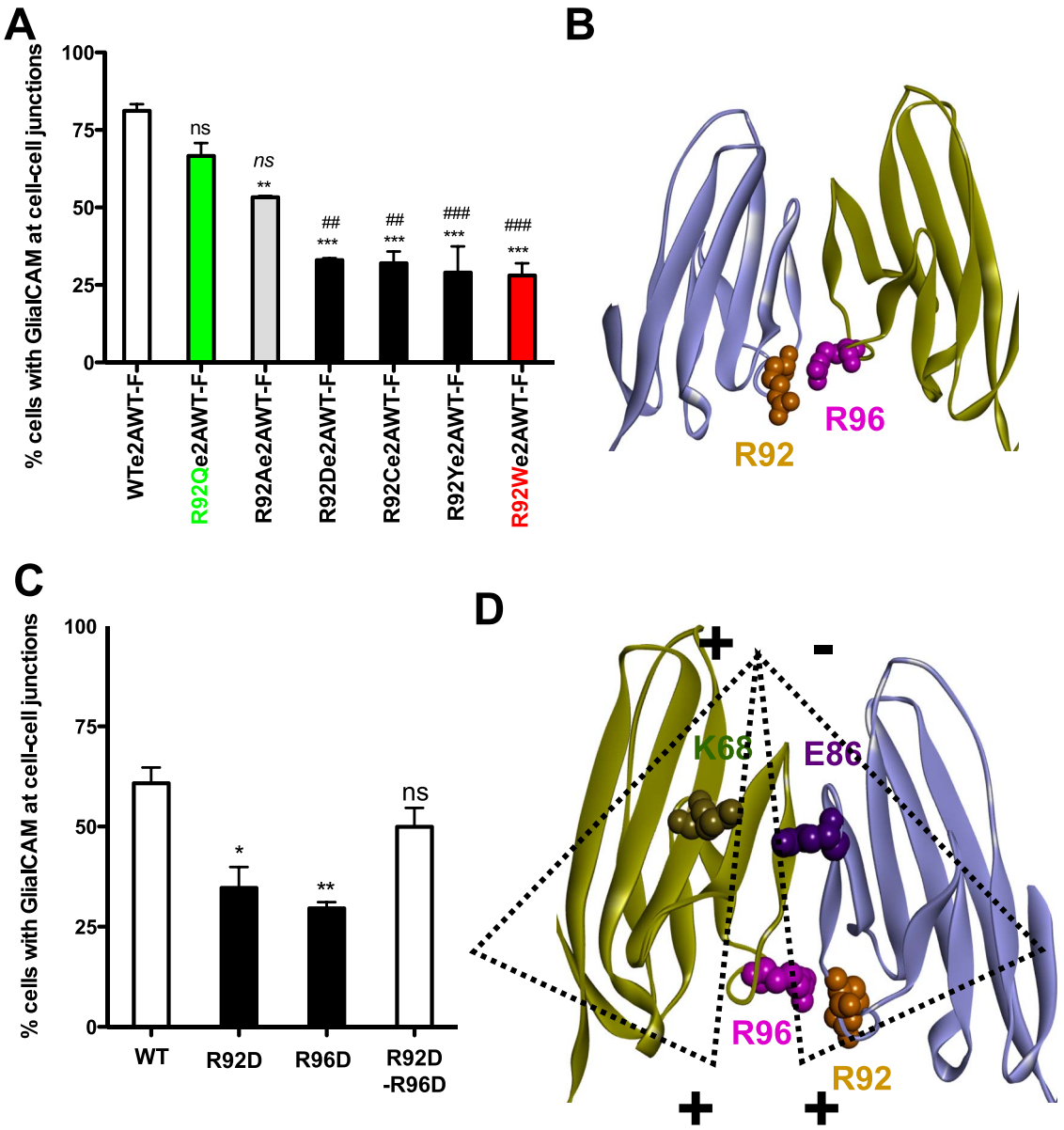

Figure 7. Structural clues on the difference between dominant and recessive mutants at the CIS interacting surface. (**A**) Biochemical dominance assay of GlialCAM WT targeting to cell–cell junctions co-expressed with different R92 mutants (left). Quantification of flag-tagged GlialCAM at cell–cell junctions (right) when co-expressed in E2A constructs with GlialCAM WT (130 cells), mutant p.R92Q (115 cells) R92A (94 cells), R92Y (115 cells), R92D (127 cells), R92C (114 cells) and p.R92W (128 cells). Graphics represent mean ± SEM. ns = no statistical differences, $^{**}P < 0.01$, $^{***}P < 0.001$ when compared with co-expression with the WT. In addition, we also compared with the mutant p.R92Q, to distinguish better between recessive and dominant mutations. ns = no statistical differences, $\#\#P < 0.01$, $\#\#\#P < 0.001$ when comparing with mutant R92Q in Bonferroni multiple comparison's test of three–four different experiments. (**B**) Structural representation of the interaction between two IgV domains in CIS, with focus on the possible interactions between the residue R92 and the residue R96. (**C**) Immunofluorescence of flag-tagged WT and GlialCAM mutants R92D, R96D or double mutant R92D-R96D, where localization at cell–cell junctions is compared with the WT protein. Quantification of percentage of cell–cell junctions in WT (235 cells), R92D (240 cells), R96D (293 cells) or R92D + R96D (278 cells). Graphics represent mean ± SEM. $^{*}P < 0.05$ and $^{**}P < 0.01$, ns = no statistical differences, in Bonferroni multiple comparison test, compared with WT. Data from three independent experiments. (**D**) A proposed model of GlialCAM IgV dimerization indicates that dimer is stabilized both by attracting charges at the top of the IgV interacting segment and by repulsive charges at the bottom.

be also dominant. We also hypothesized that the MLC2B mutants p.G89S and p.G89D may also form new interactions through new hydrogen bonds or by electrostatic effects.

As previous studies have revealed (13), efficient targeting of GlialCAM to cell–cell junctions may require multiple interactions of GlialCAM with GlialCAM forming a GlialCAM dimer in the same or in the opposite cell, but also with the cytoskeleton through the C terminus, and with MLC1 or ClC-2 through unknown interacting surfaces. Moreover, recent work has shown that GlialCAM, MLC1 and ClC-2 may form a ternary complex (23). Considering the volume of the ClC-1 channel (homologous to ClC-2) (24), in the GlialCAM dimer, there is only space for ClC-2, but not for MLC1. Thus, we suggest that GlialCAM dimers may also form lateral interactions with other GlialCAM dimers accommodating ClC-2 or MLC1 within a dimer. The presence of multiple GlialCAM dimers could explain how mutation R92C may be dominant, as the possible formation of a disulphide bridge in one of these different dimers containing two GlialCAM

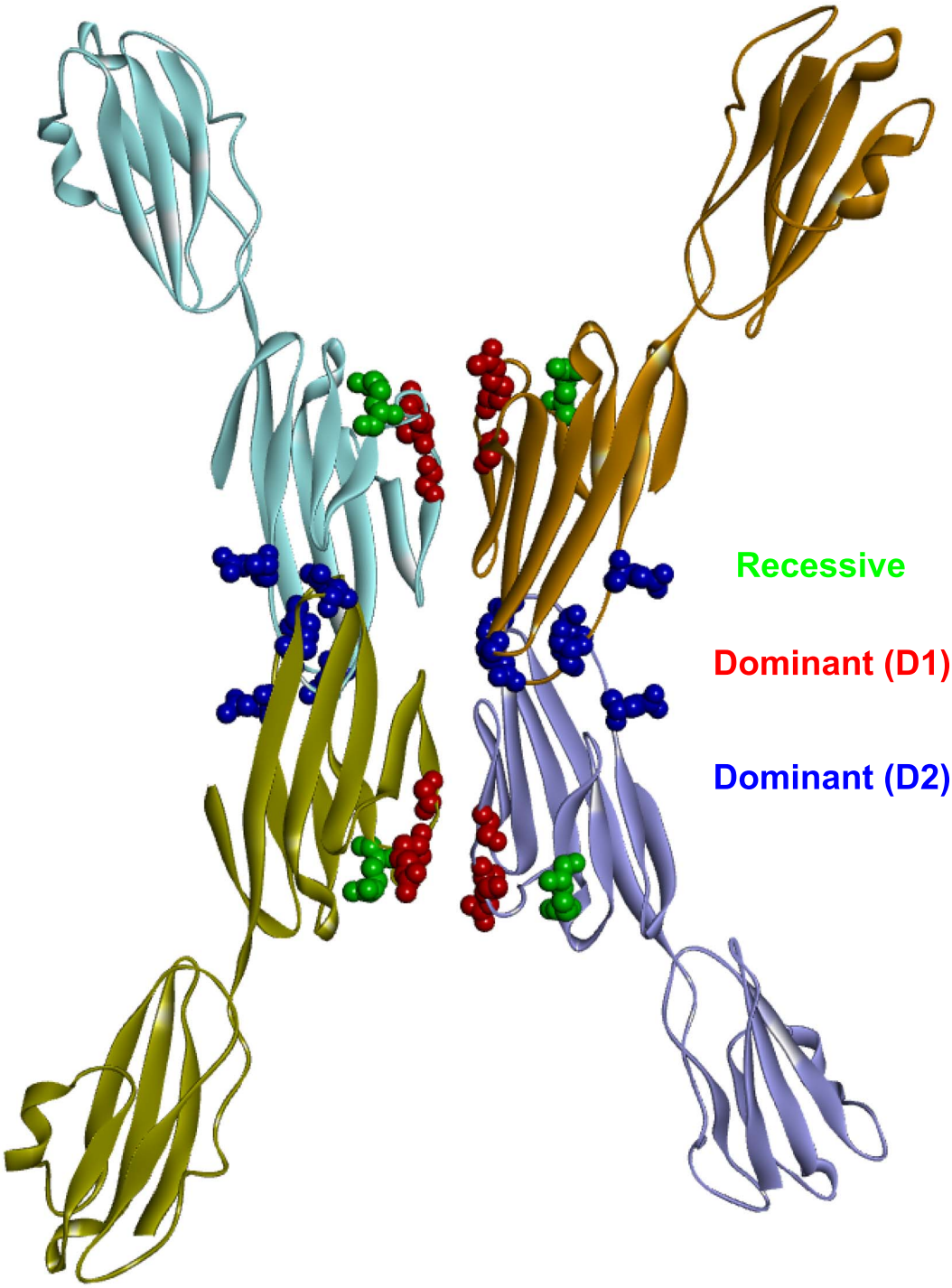

Figure 8. Summary of the structural model proposed for GlialCAM homodimers forming *cis* and *trans* interaction through different surfaces of its IgV domain. *Cis* dimerization is achieved by interactions between two opposing beta-strands of the IgV domain and *trans* interactions occurr between salient loops of both IgV domains. Residues mutated in MLC2A patients (recessive) are shown in green, D1 residues mutated in MLC2B patients are shown in red and D2 residues mutated in MLC2B patients are shown in blue. The classification of D1 and D2 mutants has been explained previously.

molecules with R92 mutated to cysteine may destabilize the overall oligomeric organization at the cell junction. It has been shown that other IgCAM molecules similar to GlialCAM have the ability to form lateral interactions that are also important for clustering through IgC2 domains (20). Therefore, maybe some mutations found in MLC2 patients in the IgC2 domain may affect GlialCAM–GlialCAM lateral interactions.

To conclude, our structural model (Fig. 8) of GlialCAM–GlialCAM dimers mediating *cis* and *trans* interactions could be used to predict the behaviour of new MLC2 mutants (22). For instance, the recently identified MLC2A mutation p.T132N is not found in an interacting surface of GlialCAM, so it may be recessive. The other new mutant identified, p.K68M, may destabilize GlialCAM–GlialCAM interaction by affecting its

electrostatic interaction with E86. Since it is not creating a new interaction, we propose it may also be recessive. In summary, this work provides new insights into the molecular basis of *GLIALCAM* mutations. We believe that this knowledge will be important to help developing therapeutic strategies for MLC patients with *GLIALCAM* mutations.

Materials and Methods

Molecular biology

Plasmids were constructed using standard molecular biology techniques employing recombinant PCR and the Multisite Gateway System (Invitrogen, Carlsbad, CA, USA). For localization studies, all GlialCAM constructs were flag tagged at their C-terminus (three flag copies) and cloned into the pCDNA3 vector. Flag tagged WT GlialCAM was co-expressed with different GlialCAM mutants by generating constructs where both cDNAs were linked to the self-cleavable 2A peptide (E2A). The sequence of the E2A peptide was: *Gly-Ser-Gly-Glu-Gly-Arg-Gly-Ser-Leu-Leu-Thr-Cys-Gly-Asp-Val-Glu-Glu-Asn-Pro-Gly*. The integrity of all cloned constructs was confirmed by sequencing. All cDNAs are from human origin. In the results section, mutations found in patients are mentioned using the genetic nomenclature (for instance p.R92W), whereas other mutants simply describe the mutation (for instance E86C).

Cell transfection

HeLa cells were grown in Dublecco's modified Eagle's medium containing (v/v) 10% foetal bovine serum (FBS, Sigma, St Louis, MO, USA) 1% glutamine and 1% penicillin/streptomycin at 37°C in a humidity controlled incubator with 5% CO_2. Cells were transiently transfected with Transfectin Lipid Reagent (Bio-Rad, Madrid, Spain) following the manufacturer's instructions (https://www.bio-rad.com/webroot/web/pdf/lsr/literature/4106254A.pdf). Experiments were performed 48–72 h after cell transfection. To assay whether a mutant was acting in a dominant manner, cells were co-transfected with GlialCAM WT (or mutant)-E2A- GlialCAM WT-flag tagged plus MLC1. This was done to maximize the percentage of GlialCAM in cell–cell junctions, as it was previously described that MLC1 improves the percentage of GlialCAM in cell–cell junctions (15). In this case, we always detect MLC1 and flag-tagged GlialCAM by immunofluorescence and performed our quantitative analyses on GlialCAM only on cells that express MLC1. To study the effect of mutations on GlialCAM trafficking, GlialCAM WT or mutant flag-tagged were transfected independently.

Immunofluorescence of transfected cells

Twenty four hour transfected HeLa cells were split and transferred onto glass coverslips in Petri dishes, and grown for further 24–48 h. Later, cells were fixed with phosphate-buffered saline (PBS) containing 3% paraformaldehyde (PFA) for 20 min, blocked and permeabilized with 10% FBS and 0.1% Triton X-100 in PBS for 2 h at room temperature (RT). Primary antibodies were diluted in the same solution and incubated 1 h at RT. The antibodies used were mouse anti-flag (1:500) (Sigma) and polyclonal rabbit anti-MLC1 (1:100) (25). Cells were washed and incubated with secondary antibodies for 2 h at RT. Coverslips were mounted in Vectashield medium (Vector Laboratories, Burlingam, CA, USA), with 1.5 µg/mL 4′,6-diamidino-2-phenylindole (DAPI, Sigma) and visualized using a DSU spinning disk confocal microscope (Olympus, Tokyo, Japan). Pairs of immunostained cells were analyzed manually to determine whether or not the staining was present in junctions, as described previously (13).

Split-TEV method

The Split-TEV assay was performed exactly as described previously (Lopez-Hernandez *et al*. 2011*b*; Capdevila- Nortes *et al*. 2012; Jeworutzki *et al*. 2012). Briefly, TEV protease was divided into two fragments: the TEV-N (residues 1–118) and the TEV-C (residues 119–242). TEV-N fragment, the TEV protease recognition site and the chimeric transcription factor GV were fused to the C-terminus of GlialCAM WT in a pCDNA3 vector containing a cytomegalovirus promoter. In addition, we fused the TEV-C fragment to the C-terminus of WT or different GlialCAM mutants. All proteins with the TEV-C fragments were cloned in a pCDNA6.2/V5-pL Dest, containing the herpes simplex virus thymidine kinase promoter, to obtain low to moderate levels of expression. The non-interacting protein 4F2hc was used as a negative control.

Cysteine crosslinking assays, western-blot and glycosylation analysis

For western blot studies, lysates were prepared by cell homogenization in PBS containing 1% Triton X-100 and protease inhibitors: 1 mM pepstatin and leupeptin, 1 mM aprotinin and 1 mM PMSF, incubated for 1 h at 4°C and centrifuged. Proteins in supernatants were quantified using the BCA Kit (Pierce, Thermo Scientific, Rockford, IL, USA) and mixed with SDS loading sample buffer (LSB4X). When processing samples of proteins that may establish disulphide bonds, samples were prepared with LSB4X without reducing agents and boiled for 3 min at 50°C. In order to confirm the disulphide-bound nature of dimeric proteins, protein extracts were treated with 100 mM DTT in SDS loading sample buffer and boiled at 95°C for 5 min.

Western blot analysis was performed as previously described (26). Membranes were incubated with primary antibodies: anti-Flag (1:500) and anti-beta actin (1:5000, Sigma) and secondary antibodies: HRP-conjugated anti-mouse (1:5000; Jackson).

Evaluation of glycosylation status of GlialCAM protein was achieved through denaturing glycosylation assays with PNGase F (New Englan BioLabs, Ipswich, UK). Protein extracts were denatured by heating at 100°C for 10 min with glycoprotein denaturing buffer and treated with PNGase F enzyme for 1 h at 37°C. Finally, treated samples were prepared with LSB4X and analyzed by western blot.

Obtention of nanobodies and minibodies against GlialCAM

The sequence of 139G1 Nb was cloned into the vector pHEN2 that included a hexa-histidine tag at the C-terminus. 139G1 Nb was produced by Hybrigenic Services SAS, Paris, France. Three rounds of phage display selection were carried out using cells expressing GlialCAM. Hybrigenics' synthetic hsd2Ab VHH library of 3.109 clones was expressed at the surface of M13 phage. Hybrigenics' phage display allowed selecting VHHs recognizing the non-adsorbed antigen in a native form. Selected VHHs were validated in non-adsorbed Phage ELISA and were then tested in FACS assay. The 139G1 nanobody plasmid was amplified in the *E. coli* WK6 strain (SBRC, Instruct Integrating Biology, Brussel), as described previously (27). In brief, 3–4 individual colonies of the 139G1 Nb were randomly picked, and those were produced as soluble His- and Capture Select C-tagged proteins (MW

12–15 kDa) in the periplasm of *E. coli*. Inducible periplasmic expression of Nb in *E. coli* WK6 strain produced milligramme amounts of > 95% pure Nb using immobilized Ni/NTA Agarose resin (Qiagen, Hilden, Germany) from the periplasmic extract of a 1-l culture. Purified Nb (2–10 mg ml^{-1}) in 20 mM Tris-Base, NaCl 150 mM, pH 7.4 were frozen in liquid nitrogen and stored at −80°C before use.

The VHH 139G1 coding sequence was inserted in pFuse plasmid (Hybrigenic Services), which included an Fc fragment of rabbit IgG2. The production of 139G1 Minibody (Mb) VHH 139G1 fused at their C-terminus to the Fc fragment of rabbit IgG2 was carried out in HEK 293 T cells. These cells were grown at 37°C in an atmosphere of 5% CO_2 in DMEM (Sigma-Aldrich, St Louis, MO, USA) supplemented with 1 mM sodium pyruvate, 2 mM L-glutamine, 100 U/ml streptomycin, 100 mg/ml penicillin and 5% (v/v) fetal bovine serum. The cells were seeded on 10 cm culture dishes and transiently transfected with 10 µg of 139G1 Mb using Trasfectin reagent (Bio-Rad, Hercules, CA, USA). At 24 h after the transient transfection, the media was exchanged for a serum-free media, and the cell supernatant was collected 1 day later. The presence of the Mb in this supernatant was confirmed by western blot using an HRP-conjugated anti-rabbit antibody (1:5000; Jackson).

Flow cytometry

For flow cytometry, cells were processed as previously described (26). Cells were transfected with the different GlialCAM IgV mutants into six-well plates. Forty-eight hours after transfection, cells were detached using Trypsin-EDTA 1X (Biological Industries, Kibbutz Beit-Hanemek, Israel) and resuspended in 500 µL of DMEM (Sigma-Aldrich, St Louis, MO, USA) supplemented with 1 mM sodium pyruvate, 2 mM L-glutamine, 100 U/ml streptomycin, 100 mg/ml penicillin and 5% (v/v) fetal bovine serum. The following antibodies were used: monoclonal anti-HepaCAM 0.5 mg/ml (1:50; R&D Systems) and the Mb developed in this work 139G1 Mb 0.015 mg/ml (1:1; Hybrigenic Services). These antibodies were added separately to each condition and incubated for 30 min at 4°C. Cells were washed once in 1 mL of 0.2% FBS in PBS and resuspended again in 100 mL of cell culture medium. The secondary antibodies used were: Alexa fluor 488 anti-mouse and Alexa fluor 488 anti-rabbit (1:20; Molecular Probes, Inc., Eugene, OR, USA). Secondary antibodies were added and further incubated for 30 min at 4°C. Cells were rinsed once more and resuspended in 1 mL of 0.2% FBS in PBS. To assess viability, propidium iodide was added to a final concentration of 1 mg/ml immediately before FACS analysis, performed with a Cytometre FACS Canto using the following filter sets: 550 bandpass (GFP) and 620/22 (PI). Untransfected cells and unstained transfected cells were used to set the compensation parameters. Data analysis was performed using DIBA software.

Incubation of cells with the 139G1 nanobody

HeLa cells transiently transfected with VFP-tagged GlialCAM WT construct were seeded on coverslips (100.000 cells) and treated with different doses of 139G1 Nb (5, 25 and 50 µg) for 24 h. Cells were then fixed with PBS containing 4% PFA for 20 min and blocked with 10% FBS in PBS for 2 h at RT. Cells were washed three times and coverslips were mounted in Vectashield medium (Vector Laboratories) with 1.5 µg/ml DAPI (Sigma). For the image acquisition, we worked with an Olympus DSU spinning disk confocal microscope. Experiments were analyzed using ImageJ. Cells incubated with 50 µg with the control nanobody 181Nb (28) were used as a negative control.

Modelling of GlialCAM monomer

A model of extracellular GlialCAM (containing the IgV and IgC2 domains) was built with HHPred (29) based on CAR structure (PDB 3JZ7; 24% SI). There are other available templates for the GlialCAM extracellular domains with 24–30% SI (e.g. 2V5T 24%, 1F97 28%, 3LAF 29%, 3JXA 30%), but none of them yielded better models. Modelling of the IgV alone (with templates 4GOS, 2PKD, 1NEU, 4K55, 3R0N), or using other modelling software (e.g. PSIPRED, genThreader, pDomThreader, pGenThreader, T-coffee), did not improve the models.

Modelling of GlialCAM cis dimer

Previous studies reported a *cis* dimer orientation that was quite conserved in other members of the CAM family (e.g. nectin-1-EC, CAR) (19). We initially explored whether GlialCAM could adopt the same *cis* dimeric orientation by superimposing two copies of the monomer model on the corresponding subunits of the CAR dimer (PDB 3JZ7).

However, mutational data and cross-linking experiments did not support the template-based dimer model, so we also modelled the *cis* dimer by docking, using the monomer model as input. We applied the standard pyDock protocol (30,31). We ran FTDock for exhaustive scanning of protein–protein orientations and then evaluated the energy of the 10 000 resulting docking poses with pyDock scoring function. We finally checked all docking models in search for those that satisfied mutational data.

Modelling of GlialCAM trans dimer

During our analysis of homologous structures, we identified a possible template for interactions, between the domains 2 and 3 of contactin (PDB 3JXA) (17). This protein has the highest sequence identity with GlialCAM extracellular domain (30% SI). Therefore, we built *trans* dimer by superimposing two copies of GlialCAM monomer model on contactin domains 2 and 3.

Supplementary Material

Supplementary Material is available at *HMG* online.

Funding

This work was supported in part by the Spanish *Ministerio de Ciencia e Innovación* (MICINN) (RTI2018-093493-B-I00 to RE) and BIO2016-79930-R to JFR. RE is a recipient of an ICREA Academia prize.

Conflict of Interest: None declared.

References

1. van der Knaap, M.S., Schiffmann, R., Mochel, F. *et al.* (2019) Diagnosis, prognosis, and treatment of leukodystrophies. *Lancet Neurol.*, **18**, 962–972.
2. van der Knaap, M.S.S., Boor, I., Estevez, R. *et al.* (2012) Megalencephalic leukoencephalopathy with subcortical cysts: chronic white matter oedema due to a defect in brain ion and water homoeostasis. *Lancet Neurol.*, **11**, 973–985.

3. Leegwater, P.A., Yuan, B.Q., van der Steen, J. *et al.* (2001) Mutations of MLC1 (KIAA0027), encoding a putative membrane protein, cause megalencephalic leukoencephalopathy with subcortical cysts. *Am. J. Hum. Genet.*, **68**, 831–838.
4. López-Hernández, T., Ridder, M.C., Montolio, M. *et al.* (2011) Mutant GlialCAM causes megalencephalic leukoencephalopathy with subcortical cysts, benign familial macrocephaly, and macrocephaly with retardation and autism. *Am. J. Hum. Genet.*, **88**, 422–432.
5. Hamilton, E.M.C., Cialdella, F., Rappard, V., Di, F. *et al.* (2018) Megalencephalic leukoencephalopathy with subcortical cysts: characterization of disease variants. *Neurology*, **90**, E1395–E1403.
6. Estévez, R., Elorza-Vidal, X., Gaitán-Peñas, H. *et al.* (2018) Megalencephalic leukoencephalopathy with subcortical cysts: a personal biochemical retrospective. *Eur. J. Med. Genet.*, **61**, 50–60.
7. Barrallo-Gimeno, A., Gradogna, A., Zanardi, I. *et al.* (2015) Regulatory-auxiliary subunits of CLC chloride channel-transport proteins. *Austral. J. Phys.*, **593**, 4111–4127.
8. Bugiani, M., Dubey, M., Breur, M. *et al.* (2017) Megalencephalic leukoencephalopathy with cysts: the *Glialcam* -null mouse model. *Ann. Clin. Transl. Neurol.*, **4**, 450–465.
9. Hoegg-Beiler, M.B., Sirisi, S., Orozco, I.J. *et al.* (2014) Disrupting MLC1 and GlialCAM and ClC-2 interactions in leukodystrophy entails glial chloride channel dysfunction. *Nat. Commun.*, **5**, 3475.
10. Capdevila-Nortes, X., López-Hernández, T., Apaja, P.M. *et al.* (2013) Insights into MLC pathogenesis: GlialCAM is an MLC1 chaperone required for proper activation of volume-regulated anion currents. *Hum. Mol. Genet.*, **22**, 4405–4416.
11. Jeworutzki, E., López-Hernández, T., Capdevila-Nortes, X. *et al.* (2012) GlialCAM, a protein defective in a Leukodystrophy, serves as a ClC-2 cl - channel auxiliary subunit. *Neuron*, **73**, 951–961.
12. Jeworutzki, E., Lagostena, L., Elorza-Vidal, X. *et al.* (2014) GlialCAM, a CLC-2 cl(−) channel subunit, activates the slow gate of CLC chloride channels. *Biophys. J.*, **107**, 1105–1116.
13. Capdevila-Nortes, X., Jeworutzki, E., Elorza-Vidal, X. *et al.* (2015) Structural determinants of interaction, trafficking and function in the ClC-2/MLC1 subunit GlialCAM involved in leukodystrophy. *Austral. J. Phys.*, **593**, 4165–4180.
14. Arnedo, T., López-Hernández, T., Jeworutzki, E. *et al.* (2014) Functional analyses of mutations in HEPACAM causing megalencephalic leukoencephalopathy. *Hum. Mutat.*, **35**, 1175–1178.
15. López-Hernández, T., Sirisi, S., Capdevila-Nortes, X. *et al.* (2011) Molecular mechanisms of MLC1 and GLIALCAM mutations in megalencephalic leukoencephalopathy with subcortical cysts. *Hum. Mol. Genet.*, **20**, 3266–3277.
16. Arnedo, T., Aiello, C., Jeworutzki, E. *et al.* (2014) Expanding the spectrum of megalencephalic leukoencephalopathy with subcortical cysts in two patients with GLIALCAM mutations. *Neurogenetics*, **15**, 41–48.
17. Bouyain, S. and Watkins, D.J. (2010) The protein tyrosine phosphatases PTPRZ and PTPRG bind to distinct members of the contactin family of neural recognition molecules. *Proc. Nat. Acad. Sci. U.S.A.*, **107**, 2443–2448.
18. Estévez, R. and Jentsch, T.J. (2002) CLC chloride channels: correlating structure with function. *Curr. Opin. Struct. Biol.*, **12**, 531–539.
19. Narita, H., Yamamoto, Y., Suzuki, M. *et al.* (2011) Crystal structure of the cis-dimer of Nectin-1. *J. Biol. Chem.*, **286**, 12659–12669.
20. Kamiguchi, H. and Lemmon, V. (2000) IgCAMs: bidirectional signals underlying neurite growth. *Curr. Opin. Cell Biol.*, **12**, 598–605.
21. Matthäus, C., Langhorst, H., Schütz, L. *et al.* (2017) Cell-cell communication mediated by the CAR subgroup of immunoglobulin cell adhesion molecules in health and disease. *Mol. Cell. Neurosci.*, **81**, 32–40.
22. Shi, Z., Yan, H.-F., Cao, B.-B. *et al.* (2019) Identification in Chinese patients with GLIALCAM mutations of megalencephalic leukoencephalopathy with subcortical cysts and brain pathological study on Glialcam knock-in mouse models. *World J. Pediatr.*, **15**, 454–464.
23. Sirisi, S., Elorza-Vidal, X., Arnedo, T. *et al.* (2017) Depolarization causes the formation of a ternary complex between GlialCAM, MLC1 and ClC-2 in astrocytes: implications in megalencephalic leukoencephalopathy. *Hum. Mol. Genet.*, **26**, 2436–2450.
24. Wang, K., Preisler, S.S., Zhang, L. *et al.* (2019) Structure of the human ClC-1 chloride channel. *PLOS Biol.*, **e3000218**, 17.
25. Teijido, O., Casaroli-Marano, R., Kharkovets, T. *et al.* (2007) Expression patterns of MLC1 protein in the central and peripheral nervous systems. *Neurobiol. Dis.*, **26**, 532–545.
26. Teijido, O., Martínez, A., Pusch, M. *et al.* (2004) Localization and functional analyses of the MLC1 protein involved in megalencephalic leukoencephalopathy with subcortical cysts. *Hum. Mol. Genet.*, **13**, 2581–2594.
27. Pardon, E., Laeremans, T., Triest, S. *et al.* (2014) A general protocol for the generation of Nanobodies for structural biology. *Nat. Protoc.*, **9**, 674–693.
28. Errasti-Murugarren, E., Fort, J., Bartoccioni, P. *et al.* (2019) L amino acid transporter structure and molecular bases for the asymmetry of substrate interaction. *Nat. Commun.*, **10**, 1807.
29. Soding, J., Biegert, A. and Lupas, A.N. (2005) The HHpred interactive server for protein homology detection and structure prediction. *Nucleic Acids Res.*, **33**, W244–W248.
30. Cheng, T.M.-K., Blundell, T.L. and Fernandez-Recio, J. (2007) pyDock: electrostatics and desolvation for effective scoring of rigid-body protein-protein docking. *Proteins*, **68**, 503–515.
31. Jiménez-García, B., Pons, C. and Fernández-Recio, J. (2013) pyDockWEB: a web server for rigid-body protein–protein docking using electrostatics and desolvation scoring. *Bioinformatics*, **29**, 1698–1699.